Efficient extraction of quantum Hamiltonians from optimal laboratory data

JM Geremia*

Physics and Control and Dynamic Systems, California Institute of Technology, Pasadena, California 91125, USA

Herschel A. Rabitz

Department of Chemistry, Princeton University, Princeton, New Jersey 08540, USA

Optimal identification (OI) is a recently developed procedure for extracting information about quantum Hamiltonians from experimental data. It employs techniques from coherent learning control to drive the quantum system such that dynamical measurements provide maximal information about its Hamiltonian. OI is an optimal procedure as initially presented; however, the data inversion component is computationally expensive. Here, we demonstrate that highly efficient global, nonlinear, map-facilitated inversion procedures can be combined with the OI concept to make it more suitable for laboratory implementation. A simulation of map-facilitated OI illustrates how the input-output maps can greatly accelerate the data inversion process.

I. INTRODUCTION

A general goal in atomic and molecular physics is to predict quantum dynamics from knowledge of the system Hamiltonian. In many applications, however, sufficiently detailed information about these Hamiltonians is still lacking. Although the capabilities of *ab initio* methods are improving, they remain unable to provide the quantitative accuracy needed to predict many quantum dynamical phenomena, and inversion of laboratory data remains the most reliable source of precision information about quantum Hamiltonians. But traditional data inversion techniques are hindered by the facts that (a) spectroscopic and collision data provide information about only limited portions of the desired interactions and (b) the relationships between quantum Hamiltonians and the corresponding observables measured in the laboratory are generally nonlinear [1].

Our recently proposed optimal identification (OI) [2,3] procedure provides an approach to Hamiltonian identification through laboratory data inversion. The principle behind OI is that it is possible to improve the information content of laboratory data by applying a tailored control field (e.g., a shaped laser pulse) while the measurements are being performed. If suitably chosen, the control field forces the data to become highly sensitive to otherwise inaccessible portions of the Hamiltonian, and it is therefore expected to greatly enhance the fidelity of the inversion.

The OI concept exploits the fact that data inversion fundamentally reveals a family, or distribution, of Hamiltonians consistent with the laboratory data [4,5]. The limiting factors that prevent typical inversion families from collapsing down to a single (i.e., completely certain) member arise from two sources. First, the finite precision of laboratory data reduces the resolving power of the measurements. Thus, multiple Hamiltonians may reproduce the data to within its experimental error. Second, most quantum observables are sensitive only to limited functional aspects (or features) of the Hamiltonian; for instance, infrared spectral lines are generally weakly dependent on high-energy regions of the repulsive barrier and the long-range structure of a molecular potential.

For a given set of data, the breadth of the inversion family provides a figure of merit for the inversion quality—a smaller family of Hamiltonians reflects greater certainty in the inversion. OI operates by attempting to drive the quantum system through dynamical states where the associated experimental errors are least compromising and where the measurements provide maximal distinguishing power between Hamiltonians. The OI algorithm embeds data inversion within a coherent learning control optimization that acts to minimize the size of the inversion family. As originally presented, this process requires a full data inversion for each trial control field, and repeatedly solving the Schrödinger equation during inversion can be computationally expensive [3]. In this paper, we demonstrate that it is possible to greatly reduce the computational component of OI by adopting map-facilitated inversion techniques [4–6] that have been specifically developed for efficiently finding global inversion families. A map is a predetermined quantitative input →output relationship which can alleviate the expense of repeatedly solving the Schrödinger equation [1].

This paper provides a detailed description of the algorithm demonstrated in Ref. [2] for extracting both internal Hamiltonian and transition dipole moment matrix elements from simulated laser pulse shaping and population data. Section II reviews the OI concept introduced in Ref. [3] and then extends this procedure to incorporate map-facilitated inversion. Section III provides a detailed description and in-depth analysis of the simulations that were presented in Ref. [2].

II. ALGORITHM

The OI algorithm operates in a manner similar to the learning-loop techniques [7] utilized in many current coherent quantum control experiments. The distinction between OI

---

*Electronic address: jgeremia@Caltech.edu

and typical control experiments lies in the optimization target: OI is guided to optimize the quality of the extracted Hamiltonian information. This goal is achieved via a learning algorithm that controls the shape of a driving laser pulse and then acquires a collection of associated dynamical observations. In practice, the control optimization is performed over a discrete set of variables (control "knobs"), $\mathbf{c} \equiv \{c_1, \ldots, c_{N_c}\}$,

$$E(t) \rightarrow E(t; c_1, c_2, \ldots, c_{N_c}) \tag{1}$$

where the space of accessible fields is defined by varying each c_i over a range $c_i^{(min)} \leq c_i \leq c_i^{(max)}$. For each trial field,

$E_k(t; \mathbf{c}_k)$, $k = 1, 2, \ldots$, a set of measurements $\Phi_k^{(lab)}$ are performed on the system. Each trial field yields M individual measurements (e.g., the populations of M different quantum states) $\Phi_k^{(lab)} = \{\Phi_{k,1}^{(lab)}, \ldots, \Phi_{k,M}^{(lab)}\}$ with associated errors $\{\varepsilon_{k,1}^{(lab)}, \ldots, \varepsilon_{k,M}^{(lab)}\}$.

Inversion is performed by adopting a discrete set of variables $\mathbf{h} = \{h_1, \ldots, h_{N_h}\}$ used to distinguish one trial Hamiltonian from another. There are many possible ways to define these Hamiltonian variables, and the best representation must be selected to suit the quantum system being inverted. In general, a sufficiently flexible description of Hamiltonian space requires a large number of variables $N_h \gg 1$. Inversion is accomplished by minimizing

$$\mathcal{J}_{inv}(\mathbf{h}; \Phi_k^{(lab)}) = \frac{1}{M} \sum_{m=1}^{M} \left\{ \begin{array}{ll} 0, & |\Phi_{k,m}^{(lab)} - \Phi_{k,m}[\mathbf{h}]| \leq \varepsilon_{k,m}^{(lab)} \\ \left\| \dfrac{\Phi_{k,m}^{(lab)} - \Phi_{k,m}[\mathbf{h}]}{\Phi_{k,m}^{(lab)}} \right\|^2, & |\Phi_{k,m}^{(lab)} - \Phi_{k,m}[\mathbf{h}]| > \varepsilon_{k,m}^{(lab)} \end{array} \right\} + \hat{K}\mathbf{h}, \tag{2}$$

where $\Phi_{k,m}[\mathbf{h}]$ is the mth ($m = 1, \ldots, M$) observable's computed value for the trial Hamiltonian $\mathbf{h}$ under the influence of the external field $E_k(t)$. Optionally, a regularization operator $\hat{K}$ acting on the Hamiltonian $\mathbf{h}$ can be used to incorporate *a priori* behavior, such as smoothness, proper asymptotic behavior, symmetry, etc., into the inverted Hamiltonian [4,8,9]. While the data error distributions are assumed to have hard bounds $\varepsilon_{k,m}^{(lab)}$ in Eq. (2), other distributions could be used as well.

The output of the inversion optimization is a set of N_s Hamiltonians $\{\mathbf{h}_1^*, \ldots, \mathbf{h}_{N_s}^*\}$ that each ideally reproduce the measured observable $\Phi_k^{(lab)}$ to within its experimental error. The upper and lower bounds of each inverted variable define the family,

$$^< h_i^* = \min_s \{h_{s,i}^*\}, \tag{3}$$

$$^> h_i^* = \max_s \{h_{s,i}^*\}, \tag{4}$$

where $h_{s,i}^*$ is the ith Hamiltonian variable from the sth member of $\mathbf{H}^*$. The uncertainty in each Hamiltonian variable Δh_i^* is quantified by the width of its corresponding solution space,

$$\Delta h_i^* = {^>h_i^*} - {^<h_i^*}, \tag{5}$$

and the width of the family for each Hamiltonian variable is used to compute the uncertainty in the full inversion $\Delta \mathbf{H}^*[E_k(t)]$,

$$\Delta \mathbf{H}^*[E_k(t)] = \frac{1}{N_s} \sum_{s=1}^{N_s} \mathcal{J}_{inv}[\mathbf{h}_s^*; \Phi_k^{(lab)}] + \alpha \frac{1}{N_h} \sum_{i=1}^{N_h} \left| \frac{2\Delta h_i^*}{^<h_i^* - {^>h_i^*}} \right|, \tag{6}$$

where $\mathbf{h}_s^*$ is the sth member of the inversion family found from $E_k(t)$ and $\mathcal{J}_{inv}$ is given by Eq. (2). The first term in Eq. (6) measures the ability of the inversion family to reproduce the data and the second measures the inversion uncertainty with $\alpha > 0$ being a coefficient that balances them.

This measure of inversion uncertainty is used to guide the control optimization where the objective is to optimize $\Delta \mathbf{H}^*$ over the space of accessible fields by minimizing the control cost function,

$$\mathcal{J}_c[E(t; \mathbf{c})] = \Delta \mathbf{H}^*[E(t; \mathbf{c})] + \beta \sum_{i=1}^{N_c} \left| \frac{c_i - c_i^{(min)}}{c_i^{(max)} - c_i^{(min)}} \right|, \tag{7}$$

where the first term reduces inversion error and the second removes extraneous field components relative to their minimum value, balanced by $\beta > 0$.

The result of the control field optimization is a set of laboratory data and its corresponding inversion results $\{E_k^*(t), \Phi_k^*, \varepsilon_k^*, \mathbf{h}_k^*\}$ that provide the best possible knowledge of the unknown Hamiltonian provided by the set of accessible optimal control fields. This inversion result provides the *optimal identification* of the quantum system with uncertainty

$$\Delta h_i^* = {^>h_i^*} - {^<h_i^*} \tag{8}$$

where ${^>h_i^*}$ and ${^<h_i^*}$ are computed using Eqs. (3) and (4) for the optimal data.

A. Map-facilitated inversion

The most expensive operation in OI is the many solutions of Schrödinger's equation required in the inversion component of the algorithm. The map-facilitated inversion aims to alleviate this costly operation. Computing quantum observables $\Phi_k[\mathbf{h}]$ from a given Hamiltonian $\mathbf{h}$ and control field $E_k(t;\mathbf{c}_k)$ defines a forward map

$$f:(\mathbf{h};E_k) \rightarrow \Phi_k[\mathbf{h}] \qquad (9)$$

that is parametrized by the control field $E_k(t)$. In the initial presentation of OI, this map is explicitly evaluated each time a trial Hamiltonian is tested to determine if it is consistent with the laboratory data. However, it has recently been found that it is possible to pre-compute this map to high accuracy by sampling $f(\mathbf{h};E_k)$ for a representative collection of Hamiltonians.

Although it is generally impossible to resolve f on a full grid in $\mathbf{h}$ space due to exponential sampling complexity in $N_h \gg 1$ dimensions, it has been found [1] that an accurate nonlinear map can often be constructed using the functional form

$$f(\mathbf{h};E_k) = f_0(E_k) + \sum_{i=1}^{N_h} f_i(h_i;E_k) + \sum_{i<j}^{N_h} f_{ij}(h_i,h_j;E_k) + \cdots$$
$$+ f_{1\ldots N_h}(h_1, \ldots, h_{N_h};E_k). \qquad (10)$$

Equation (10) belongs to a family of multivariate representations used to capture the input→output relationships of many high-dimensional physical systems [1,10–17]. The functions contributing to the map expansion in Eq. (10) represent projections of the full N-dimensional Hamiltonian →observable relationship onto the space of lower-dimensional functions. This mapping is unlike typical basis expansions and there are several alternative methods for determining the functions in Eq. (10). Here, we consider the *cut* technique [10]. The constant term $f_0(E_k)$ is defined as

$$f_0(E_k) \equiv f(\bar{\mathbf{h}};E_k) \qquad (11)$$

where $\bar{\mathbf{h}}$ is a nominal value of the input variables referred to as the *cut center* [1]. The first-order functions $f_i(h_i;E_k)$ depend only upon a single variable h_i and are defined as

$$f_i(h_i;E_k) \equiv f(\bar{h}_1,\overline{\ldots},h_i,\overline{\ldots},\bar{h}_N;E_k) \qquad (12)$$

where the notation $\overline{\ldots}$ indicates that corresponding variables are given by their cut-center value $\bar{\mathbf{h}}$. Similarly, the functions $f_{ij}(h_i,h_j;E_k)$ depend upon two variables h_i and h_j and are given by

$$f_{ij}(h_i,h_j;E_k) \equiv f(\bar{h}_1,\overline{\ldots},h_i,\overline{\ldots},h_j,\overline{\ldots}\bar{h}_N;E_k). \qquad (13)$$

It has been shown that Eq. (10) converges to low order $L \ll N_h$ for many Hamiltonian→observable maps. A low-order, converged map expansion can be truncated after its last significant order without sacrificing accuracy or nonlinearity. The surviving map functions are learned by sampling them on a grid over their comparatively small number of independent variables. Once the map is learned, the process

of solving the Schrödinger equation for an arbitrary Hamiltonian, characterized by the variables $\mathbf{h}$, is accomplished equivalently by evaluating $f(\mathbf{h};E_k)$, which can be performed extremely efficiently. Greater detail regarding how the expansion functions are generated and evaluated can be found in previous papers [1,6,17].

In map-facilitated OI, the computationally expensive process of computing $\Phi_k[\mathbf{h}]$ in Eq. (2) is replaced by evaluating the map function $f(\mathbf{h};E_k)$, which provides a high-speed replacement for the Schrödinger equation. The map (or potentially multiple maps if this is necessary to ensure sufficient accuracy [4]) must be constructed as a preliminary step prior to initiating the inversion optimization. Since map construction requires knowledge of the control field, it may not be possible to precompute all of the maps prior to executing the full OI loop. Instead, a new map will generally need to be constructed for each trial laser pulse.

The computational savings afforded by map-facilitated inversion is problem dependent. However, in general, the benefits of maps become more dramatic for increasingly difficult quantum inversions. This can be seen as follows. Constructing the map requires a small, fixed number of evaluations of the Schrödinger equation. For example, first-order truncation of Eq. (10) requires NS evaluations, where S is the number of sample points used to numerically resolve each of the functions $f_i(h_i;E_k)$. Similarly, a second-order map requires $O(N^2S^2)$ evaluations, where each $f_{ij}(h_i,h_j;E_k)$ is sampled on an $S \times S$ grid. Once the overhead of map construction is completed, further calculation of quantum observables for additional trial Hamiltonians can be accomplished at negligible cost. Although it is not generally possible to predict the number of times that Eq. (2) must be evaluated during the inversion optimization, it has been empirically shown that this number will normally greatly exceed the cost of map construction [3].

III. ILLUSTRATION

The map-facilitated OI algorithm was simulated for an eight-level Hamiltonian [18] chosen to resemble vibrational transitions in a molecular system where the objective was to extract optimal information about the molecular Hamiltonian H and dipole moment μ for a system having the total Hamiltonian

$$\hat{H} = H - \mu E_k(t). \qquad (14)$$

The control fields have the form

$$E_k^{(j)}(t) = \exp\left(\frac{-(t-T/2)^2}{2s^2}\right)\sum_l A_l^{(j)}\cos(\omega_l t + \theta_l^{(j)}) \qquad (15)$$

where the ω_l are the resonance frequencies [18] of H, $A_l^{(j)}$ their corresponding amplitudes, and $\theta_l^{(j)}$ their associated phases. Control field noise was modeled as parametric uncertainties in the A_l and θ_l,

$$A_l^{(j)} = (1 + \gamma_{A_l}^{(j)})A_l, \quad \theta_l^{(j)} = (1 + \gamma_{\theta_l}^{(j)})\theta_l \qquad (16)$$

where different random values between $\pm\varepsilon^{(fld)}$ were chosen for $\gamma_{A_l}^{(j)}$ and $\gamma_{\theta_l}^{(j)}$ for each pulse.

The OI simulation involved learning the matrix elements of the Hamiltonian $H_{pq} = \langle p|H|q \rangle$ and dipole moment, $\mu_{pq} = \langle p|\mu|q \rangle$ for a chosen basis $|p\rangle$, $p=1,\ldots,8$ [19]. Simulated laboratory data was generated by propagating the initial wave function under the influence of the applied control field from its initial state and computing the populations (in the chosen basis $|p\rangle$) at various times t_q during the evolution. Each population "measurement" was averaged over $D=100$ replicate observations for a collection of noise-contaminated fields $\{E_k^{(j)}(t)\}$, $j=1,\ldots,D$, centered around the nominal field $E_k(t)$ to simulate experimental uncertainty in the laser pulse-shaping process. Measurement error $\varepsilon^{(lab)}$ was introduced into the population observations according to

$$\Phi_{k,m}^{(lab)} = \langle (1+\rho_{ij})p_i(t_q;[E_k^{(j)}(t)])\rangle_{j=1,\ldots,D} \qquad (17)$$

where the ρ_{ij} were chosen randomly between $\pm\varepsilon^{(obs)}$, the relative error in each population observation. A different random value ρ_{ij} was selected for every simulated measurement.

Equation (7) was minimized over $\mathbf{c}=\{A_l,\theta_l\}$ using a steady state genetic algorithm (GA) with a population size of 30, a mutation rate of 5%, and a crossover rate of 75%. The pulse parameters were chosen to be $T=1.0$ ps and $s=200$ fs, the amplitudes A_l were allowed to vary over [0,1] V/Å, and the phases were allowed to vary over [0, 2π] rad. The laboratory measurement error was assumed to be $\varepsilon_k^{(lab)}=2\%$, the field error $\varepsilon^{(fld)}=1\%$, and the observation times t_q were uniformly spaced over the evolution period (i.e., the time between observations was $\Delta t = T/Q$ with $Q=1$, 2, or 4). At each time, the full set of eight populations was measured. The parameters α in Eq. (6) and β in Eq. (7) were ramped from 1×10^{-4} to 1×10^{-2} over the GA evolution, although the optimization was insensitive to the exact choices of α and β. Typically ~ 50 generations, or approximately 800 trial fields, were needed for GA convergence.

Global inversion to identify the Hamiltonian family corresponding to the data, $\Phi_k^{(lab)}$, was performed by minimizing Eq. (2) using a map-facilitated inversion algorithm. For each inversion, the family of consistent Hamiltonians was identified using a steady state GA with a cross over rate of 70% and a mutation rate of 5%. The trial family size was $N_s = 500$ and the GA population size was $N_p = 100$. The Hamiltonian-space map variables h_i were the matrix elements of the molecular Hamiltonian H_{mn} and the the dipole μ_{mn}. For the eight-level system, there were 36 Hamiltonian elements (symmetric, upper triangle including the diagonal) and 28 transition dipole moments (symmetric, upper triangle without the diagonal) producing an $N_h = 64$-dimensional map. All maps were constructed to first order, $L=1$, and $S=6$ sample points were used to resolve each map function for interpolation. The Hamiltonian-space domain extended $\pm 30\%$ around its nominal value (each matrix element was assumed known to $\pm 15\%$ prior to the present identification). Typical map construction required an average of 84 s to perform on an SGI MIPS single processor machine, and map-facilitated inversion required an average of 51 s to converge. A single evaluation of the Hamiltonian→population map typically required ~ 1 ms, while a similar solution of the

Schröinger equation for this system took ~ 2 s. This difference is the origin of the savings associated with map-facilitated OI.

The performance of the map-facilitated OI algorithm was assessed with the following four tests.

(A) An OI was performed using populations measured at $Q=1$ time, $t_1=T$, producing eight observations for the 64 unknowns.

(B) An OI was performed using populations measured at $Q=2$ times, $t_1=T/2$ and $t_2=T$, producing 16 observation for the 64 unknowns.

(C) An OI was performed using populations measured at $Q=4$ times, $t_q=qT/4$, $q=1,\ldots,4$, producing 32 observations for the 64 unknowns.

(D) A conventional inversion (with a randomly selected field) was performed using populations sampled at $Q=25$ times, $t_q=qT/25$, $q=1,\ldots,25$, producing 200 observations for the 64 unknowns.

The power spectra of the optimal control fields for the $Q=$ 1, 2, and 4 OI inversions are shown in Fig. 1 along with a graphical depiction of the OI error Δh_i^*. For a single time sample, $Q=1$, the overall inversion error, computed as the average, $2\langle \Delta h_i^*/(^{<}h_i^* + ^{>}h_i^*)\rangle$, was found to be 3.67%. Figure 1(a) shows that the majority of the error was contained in and around the diagonal elements of H (note that the Hamiltonian is not diagonal in the chosen basis $|p\rangle$). The average relative error in the dipole, 0.9413%, was significantly smaller, and the majority of dipole uncertainty appeared in the $v \rightarrow v+2$ elements. The inversion error for the two-point, $Q=2$, OI demonstration was reduced to 2.910% for the molecular Hamiltonian. Again, the majority of the inversion uncertainty resides in the diagonal elements of H. The transition dipole moment elements also improved with an overall average uncertainty of 0.6270%.

The inversion error Δh_i^*, for a simulated OI utilizing data at $Q=4$ times is essentially eliminated. The average uncertainty in both the molecular Hamiltonian elements and in the transition dipoles is an order of magnitude smaller than the simulated error in the data, $\varepsilon_k^{(lab)}=2\%$. The most dramatic demonstration of the OI's capabilities is seen by comparing Figs. 1(c) and 1(d). The plot in Fig. 1(d) represents a conventional inversion, performed using a randomly selected field and $Q=25$ time samples, compared to $Q=4$ for OI. The conventional inversion therefore had access to $M=200$ data points while the map-facilitated OI demonstration had only $M=32$. Despite what would appear to be a significant advantage in the amount of available data, the conventional inversion displays greater than two orders of magnitude more error. The conventional dipole moment inversion produced an average uncertainty of 19.5% and the precision in the molecular Hamiltonian was 28.1%. The map-facilitated OI found a control field and associated data that essentially prevented the laboratory noise from propagating into the identified Hamiltonian information.

IV. CONCLUSION

We have presented simulated experimental data that demonstrate the utility of map-facilitated optimal identification
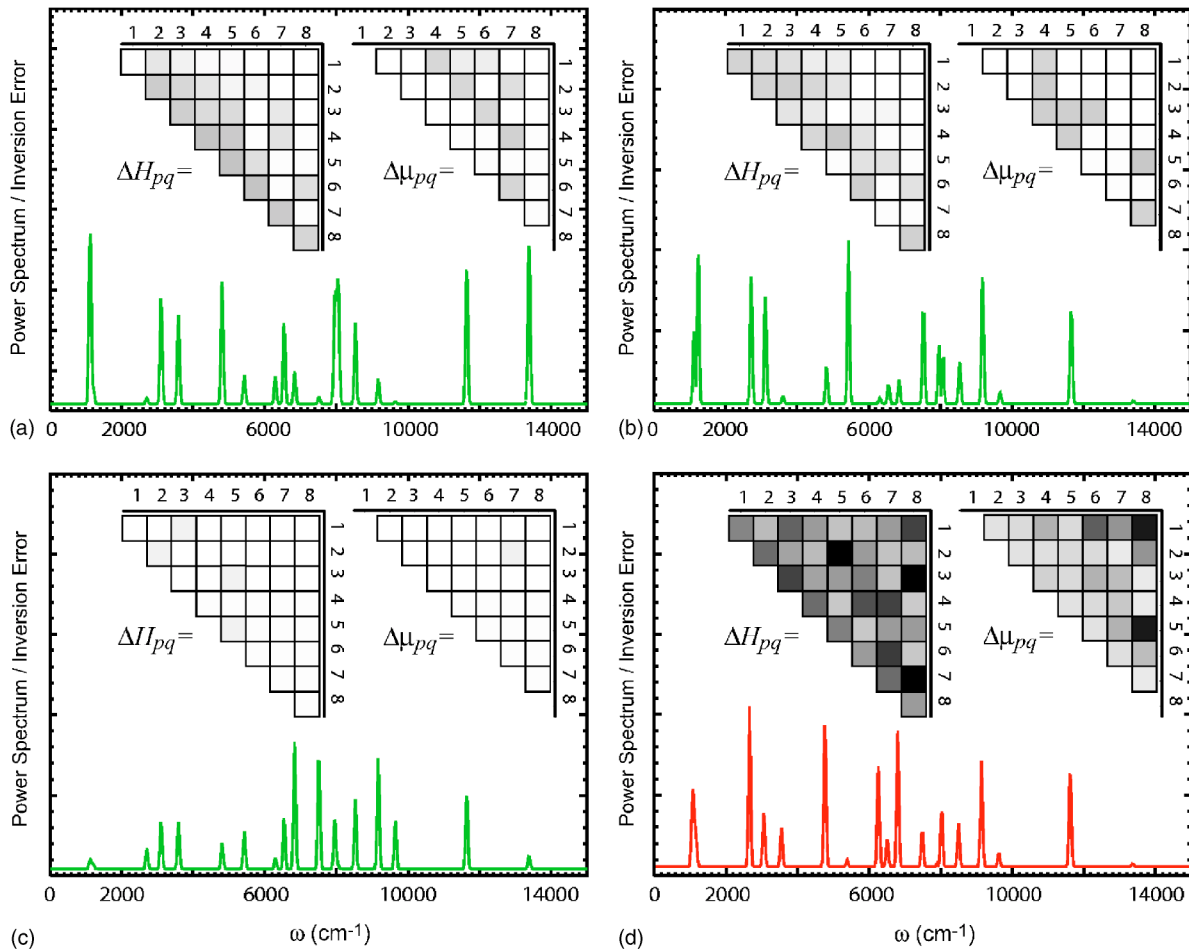
FIG. 1. (Color online) comparison of optimal versus conventional Hamiltonian identification. In plots (a)–(c) the identification error (darker shading implies larger inversion error) respectively reflects OI's performed using one, two, and four samples of the populations during the wave packet evolution. Increasing the number of data points available to the OI process improves the quality of the extracted Hamiltonian. Plot (d) represents a conventional identification where the populations were sampled 25 times during the time evolution. Despite using significantly fewer data, OI obtained higher-quality Hamiltonian information.

for the real-time laboratory identification of quantum Hamiltonians from dynamical physical observable data. Our demonstration of the algorithmic savings afforded by maps utilized a relatively simple eight-level quantum system. However, it is essential to realize that the benefit of map-facilitated inversion will be even more dramatic for higher-dimensional problems. For instance, for high-accuracy propagation of the time-dependent Schrödinger equation, it is typical for the computational complexity to scale at least as fast as N^3, due to the need to diagonalize the Hamiltonian. If a first-order map can be utilized, then the speedup will scale roughly quadratically in the number of evaluations of Eq. (2) necessary for inversion. Moreover, map construction and evaluation is highly suited for massive parallel processing schemes. In this simple demonstration of map-facilitated OI, it was possible to improve the computational efficiency of data inversion by more than an order of magnitude compared to the initial presentation of the OI concept [2]. Much greater savings should be expected for more sophisticated data inversions. This increased efficiency is ultimately expected to aid, if not be essential for, the practical implementation of OI.

[1] J. Geremia, C. Rosenthal, and H. Rabitz, J. Chem. Phys. **114**, 9325 (2001).

[2] J. Geremia and H. A. Rabitz, Phys. Rev. Lett. **89**, 263902 (2002).

[3] J. Geremia and H. A. Rabitz, J. Chem. Phys. **118**, 5369 (2003).

[4] J. Geremia and H. Rabitz, Phys. Rev. A **64**, 022710 (2001).

[5] J. Geremia and H. Rabitz, Phys. Rev. A **67**, 022117 (2003).

[6] J. Geremia and H. Rabitz, J. Chem. Phys. **115**, 8899 (2001).

[7] R. Judson and H. Rabitz, Phys. Rev. Lett. **68**, 1500 (1992).

[8] K. J. Miller, Math. Anal. **1**, 52 (1970).

[9] T.-S. Ho and H. Rabitz, J. Chem. Phys. **90**, 1519 (1989).

[10] O. Alis and H. Rabitz, J. Math. Chem. **25**, 197 (1999).

[11] H. Rabitz, O. Alis, J. Shorter, and K. Shim, Comput. Phys. Commun. **11**, 117 (1999).

[12] J. I. Shorter and H. Rabitz, Geophys. Res. Lett. **27**, 3485 (2000).

[13] J. Shorter, P. Ip, and H. Rabitz, J. Phys. Chem. A **36**, 7192 (1999).

[14] H. Rabitz and K. Shim, J. Chem. Phys. **111**, 1940 (1998).

[15] K. Shim and H. Rabitz, Phys. Rev. B **58**, 1940 (1998).

[16] H. Rabitz and K. Shim, J. Chem. Phys. **111**, 10 640 (1999).

[17] J. Geremia, E. Weiss, and H. Rabitz, Chem. Phys. **267**, 209 (2001).

[18] $\omega_{12}=1800.19$, $\omega_{23}=1620.56$, $\omega_{34}=1440.92$, $\omega_{45}=1261.29$, $\omega_{56}=1081.65$, $\omega_{67}=902.016$, and $\omega_{78}=722.38$ cm^{-1}.

[19] In practice, the basis functions could be any complete set appropriate for the system.